Document must be opened with Adobe to view all ABS amendments.

machines

FILED BY ABS FOR REFERENCE ONLY

MDPI

Article

Study on Dynamic Behaviors of Hypoid Gears Under Variable Tidal Current Energy Harvesting Conditions

Dequan Huang [1], Yan Li [2], Xingyuan Zheng [3,4] and Gang Li [5,*]

1 School of Equipment Manufacture, Zhenjiang College, Zhenjiang 212028, China; max-huang@zjc.edu.cn
2 School of Mechanical Engineering, University of Shanghai for Science and Technology, Shanghai 200093, China; 221170121@st.usst.edu.cn
3 College of Mechanical and Vehicle Engineering, Chongqing University, Chongqing 400044, China; zhengxingyuan@cqu.edu.cn
4 Department of Mechanical Engineering, University of Utah, Salt Lake City, UT 84112, USA
5 Michael W. Hall School of Mechanical Engineering, Mississippi State University, Starkville, MS 39762, USA
* Correspondence: gli@me.msstate.edu

Abstract: This study investigates dynamic behaviors of hypoid gear rotor systems under variable tidal current energy harvesting conditions through numerical simulations and experimental validation. The study examines dynamic responses of a hypoid gear rotor system induced by cyclical tidal current variations, which generate fluctuating loads and bidirectional rotational speeds in tidal energy conversion systems. Two hypoid gear pairs, modified through precise manufacturing parameters, are evaluated to optimize tooth contact patterns for bidirectional tidal loading conditions. A coupled torsional vibration model is developed, incorporating variable transmission error and mesh stiffness. Experimental validation of dynamic performances of hypoid gear pairs was conducted on a bevel gear testing rig, which can measure both torsional and translational vibrations across diverse tidal speed profiles. The experimental results demonstrate that second-order primary resonances exhibit heightened vibration intensity during flow-reversal phases. This phenomenon has significant implications for system power efficiency and acoustic emissions. The findings extend the current understanding of hypoid gear optimization for tidal energy-harvesting applications.

Keywords: hypoid gears; dynamic behaviors; transmission error; mesh stiffness; tidal current energy

check for updates

Academic Editors: Ciro Santus and Massimiliano De Agostinis

Received: 20 January 2025
Revised: 20 February 2025
Accepted: 21 February 2025
Published: 24 February 2025

Citation: Huang, D.; Li, Y.; Zheng, X.; Li, G. Study on Dynamic Behaviors of Hypoid Gears Under Variable Tidal Current Energy Harvesting Conditions. *Machines* **2025**, *13*, 178. https://doi.org/10.3390/machines13030178

Copyright: © 2025 by the authors. Licensee MDPI, Basel, Switzerland. This article is an open access article distributed under the terms and conditions of the Creative Commons Attribution (CC BY) license (https://creativecommons.org/licenses/by/4.0/).

See ABS Houston, TX Letter ref VC 1067825 dated 14-Aug-2026

1. Introduction

Hypoid gears serve as critical power transmission components in tidal current energy converters (TCECs), where they facilitate the conversion of bidirectional tidal flows into rotational mechanical energy [1]. In tidal energy applications, these gears encounter distinct challenges due to the cyclical nature of tidal current loading and the periodic flow reversals characteristic of tidal environments [2]. A cross-axis hypoid gear pair in a TCEC enables optimal spatial configuration of the power take-off system between a horizontal-axis turbine and a vertically mounted generator [3]. While conventional performance metrics such as transmission error (TE), tooth root strength, and surface wear remain crucial considerations, dynamic behaviors of hypoid gears under variable tidal current conditions introduce additional complexities due to bidirectional loading patterns. The time-varying TE and mesh stiffness (MS) function as primary internal excitation sources, whose characteristics are significantly influenced by the predictable yet varying loads and

Document must be opened with Adobe to view all ABS amendments.

reversing operational speeds inherent in TCECs [4]. Variations in TE and MS parameters, amplified by tidal current fluctuations and flow reversals, can induce complex dynamic behaviors in the rotor system's speed and load responses across different tidal cycles. These dynamic behaviors are further complicated by variations in tooth contact conditions, which emerge from micro-scale deviations in gear tooth form geometry and become particularly critical during tidal flow transitions and reversal periods. Within tidal energy applications, multiple gear tooth contact patterns may manifest across different hypoid gear pairs of identical design specifications. These are attributable to manufacturing tolerances and machining parameter variations, which become especially significant under bidirectional loading. Preventing edge-tooth contact during flow reversals is particularly important in TCECs. This necessitates comprehensive inspection protocols for hypoid gears prior to deployment in tidal environments, as such contact patterns could induce severe vibrations in the rotor system under cyclical tidal loading conditions. Hypoid gear pairs enable efficient mechanical power transmission between intersecting shafts in TCECs, converting the high-torque, low-speed rotations of tidal turbines into optimized generator inputs through precision-engineered tooth geometry and mesh characteristics. Dynamic behaviors of hypoid gear pairs of TCECs under bidirectional tidal loading conditions significantly influence their power conversion efficiency and operational reliability. It is essential for rigorous analysis of gear dynamics and transmission error of hypoid gear pairs under TCEC operational conditions to advance the performance of tidal energy harvesting technologies.

Recent studies on TCECs have predominantly focused on their hydrodynamic performances and structural reliability, with limited attention to drivetrain dynamics. Zhang et al. [5] studied unsteady effects on hydrodynamic performances of a horizontal-axis tidal turbine system, including bevel gears and a gearbox. Power fluctuations and weak characteristics of a TCEC were analyzed under wave-current interactions in [6], but neither addressed those influences on its mechanical transmission system. Chen and Wu [7] presented a comprehensive review of hybrid wave-tidal technologies, highlighting the need for improved power take-off systems, e.g., gearboxes, but without detailed expectations of gear dynamics. Avalos et al. [8] considered gearbox integration in wave energy converters. Glennon et al. [9] focused on composite blade testing methodologies for operational life prediction, emphasizing the critical need for mechanical component reliability in marine environments. These studies demonstrated a research gap regarding gear system dynamics under bidirectional tidal loading conditions, particularly concerning the interrelationship between tooth contact patterns, TE, and MS of drivetrains in TCECs under variable flow speed conditions.

Researchers assumed that the time-varying TE and MS are the prominent, exciting sources for the gearing systems. Many researchers specialized their studies on TE and MS to evaluate dynamic performances of their interest through static performances of the gearing system. Hypoid gears have much more complex tooth surface geometry, typically quasi-conjugated, than that of involute gears. Extensive research work in recent decades found it difficult to carry out the loaded tooth contact analysis (LTCA) of hypoid gears by a purely analytical approach to obtain exact solutions for load distribution, tooth contact deformation, tooth bending and shear, TE, and MS by certain formulas based on intermediate results. In all cases, the finite element (FE)-based semi-analytical LTCA approach is significantly developed, and it is powerful enough to give the desired results in the past decade, benefiting from the computational efficiency. Wang et al. [10] proposed a methodology to avoid trial and error in obtaining a satisfied design of hypoid gears, and the FE-based semi-analytic LTCA is applied in their work to calculate the bending stress of the tooth root. Liu et al. [11] investigated the impact of work-holding equipment errors on contact characteristics of face-hobbed hypoid gears and a mathematical model considering

See ABS Houston, TX Letter Ref. No. 10071825 dated 11 Aug-2026

Document must be opened with Adobe to view all ABS amendments.

both radial and angular eccentric errors. Liang et al. [12] investigated the effects on the tooth contact characteristics for the face-hobbed hypoid gears under different blade sections, and the contact pattern is compared between the linear, circular, and polynomial blades based on the FE tooth contact model. Cooley [13] proposed two determining approaches for spur gears mesh stiffness, average slope, and local slope using the FE method and a local slope difference formula for dynamic studies. In addition to the FE model, other researchers searched for numerical solutions to loaded transmission error (LTE) of hypoid gears. Huang et al. [14] used the conjugate approach to frictional loss and surface wear studies of hypoid gears. Simon [15] presented a novel hypoid gear grinding method that combines generating and Waguri motions, which can model the tooth surface roughness by considering spherical grinding wheel grains. This method achieved mapping the 3D topography to both pinion and gear tooth surfaces through their respective motions and investigating how grain size and motion relationships influence the resultant surface roughness characteristics. Liu et al. [11] used a quasistatic LTCA method to investigate contact characteristics and gear geometry with radial and angular eccentric errors.

Concerning dynamic studies of hypoid gears, researchers developed many dynamic models and explored the influence of various factors on dynamic performances. Shi et al. [16] presented a dynamic model for hypoid gears, considering the influences of dynamic MS due to time-variable contact loads. Liu et al. [17] proposed a semi-analytical LTCA method for spiral bevel gears that integrated ease-off surface computation with high-precision virtual generating tooth surfaces. Wang et al. [18] proposed a general nonlinear time-varying torsional model of hypoid gears to investigate dynamic behaviors, and typical behaviors reported in spur gears were observed, jump discontinuities, subharmonic and chaotic states from the computational results. Karagiannis et al. [19] proposed an alternative formulation for dynamic transmission error (DTE) of hypoid gears. Mohammadpour et al. [20] studied the coupling relationship between dynamics and tribology in vehicle differential hypoid gears. Athanasopoulos et al. [21] presented a sliding and rolling speed calculation method along the full path of contact on a meshing tooth surface of hypoid gears. Song et al. [22] proposed a hybrid dynamic model to investigate hypoid gears coupled with off-sized bearing rollers. Huangfu et al. [23] investigated the effects of tooth modifications on dynamic characteristics of thin-rimmed gears under surface wear conditions to optimize load distribution and reduce vibration throughout the wear process. Zheng et al. [24] presented an analytical approach to modeling the MS of high-speed spur gears, considering the centrifugal effect and its influence on gear deformation and load sharing. Li and Zhu [25] proposed a loaded contact pattern optimization method for hypoid gears, considering high-order TE functions and face-milling machine-tool settings. The integration of these diverse research efforts provides a comprehensive understanding of the current state of the field. An et al. [26] focused on improving load capacity and minimizing the effects of misalignment through development of a point contact model featuring normal cross-sectional circular arc tooth profiles. Shen et al. [27] investigated the fault mechanism and dynamic characteristics of planetary gears with gear wear and analyzed the impacts of wear on MS, TE, and gear backlash of gear tooth profiles. A dynamic model incorporating wear-related factors was developed to analyze the influences of wear on planetary gear vibration responses. Yi et al. [28] proposed a nonlinear dynamic model for spur gear systems that accounts for time-varying behaviors of pressure angle and gear backlash, providing a more realistic representation of gear dynamics and potentially influencing system stability and tooth impact states. Wei et al. [29] studied dynamic characteristics of spur gear systems with uncertain parameters, such as MS and support stiffness.

This study investigates the dynamic behavior variations between two hypoid gear configurations under distinct tooth contact conditions specifically designed for tidal current

See ABS Houston, TX Letter ref: 1006071825 dated 14-Aug-2025

Document must be opened with Adobe to view all ABS amendments.

energy harvesting applications. The logical diagram of the simulation calculation that yields the load and speed responses is shown in Figure 1. Experimental tests for hypoid gear dynamics are conducted in the meantime and compared to the simulation.

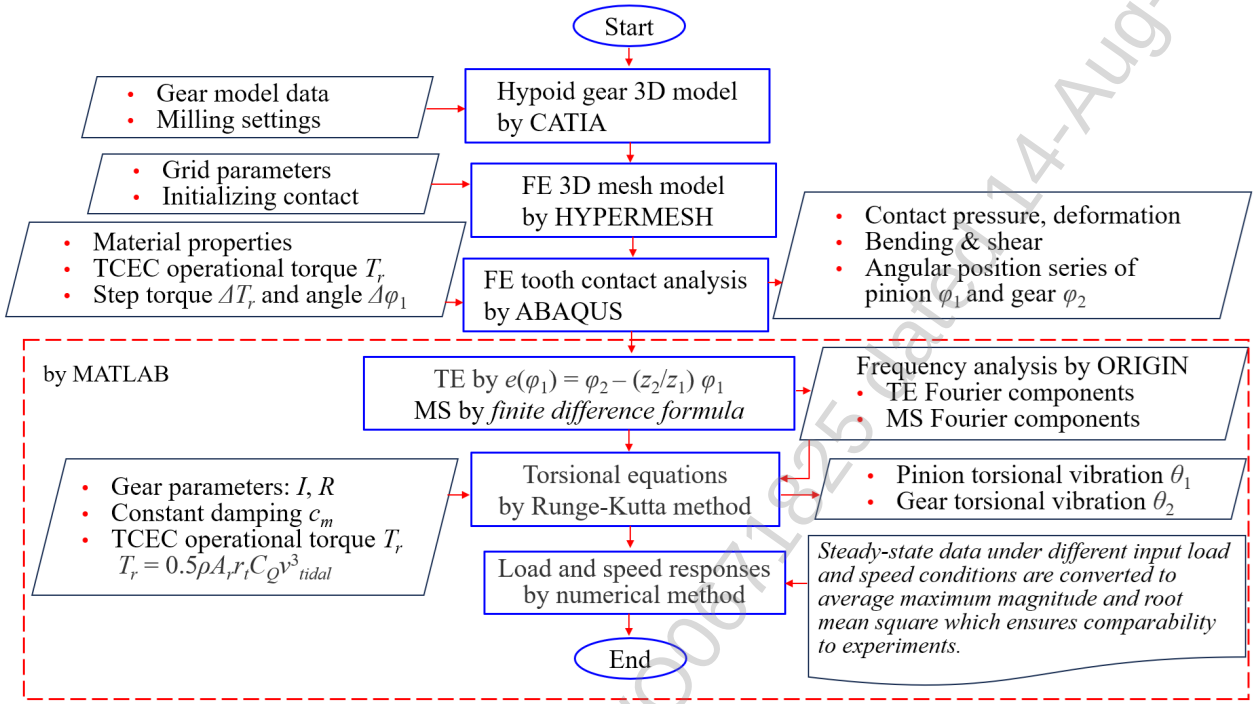

Figure 1. Logic diagram of dynamic behavior analysis for hypoid gears in TCECs

The baseline hypoid gear design, adapted from a commercial vehicle transmission, is modified for bidirectional tidal flows, featuring two gear pairs produced under different milling parameters. One pair is optimized for tidal applications, while the other provides marginal edge contact to assess system sensitivity. A comprehensive nonlinear dynamic torsional model is developed that incorporates the time-varying TE and MS parameters derived from the FE-based LTCA model, specifically accounting for bidirectional loading conditions of tidal current variations. Dynamic responses under variable tidal loading conditions are numerically solved using the Runge–Kutta method, with particular attention to behaviors during flow-reversal phases. Experimental validation is performed with a bevel gear pair testing rig that uses high-precision rotary encoders to measure torsional vibrations of both the pinion and gear, along with triaxial accelerometers to capture the full dynamic response under simulated tidal flow conditions. Numerical and experimental results are systematically analyzed to evaluate the influence of tooth contact patterns on system performance under variable tidal current conditions, leading to significant insights for optimizing hypoid gear designs in tidal energy harvesting applications. This study advances the field through three key innovations: (1) development of a coupled torsional-translational dynamic model that incorporates time-varying TE and MS under bidirectional variable tidal loading conditions; (2) experimental validation using purpose-built testing apparatus capable of measuring both torsional and translational vibrations across variable tidal speed profiles; and (3) quantitative characterization of the relationship between tooth contact patterns and system dynamics during flow-reversal phases, particularly regarding second-order primary resonances and their implications for power conversion efficiency.

See ABS Houston, TX Letter Ref WQ08/1825 dated 14-Aug-2025

Document must be opened with Adobe to view all ABS amendments.

2. Power Conversion Modeling of Drivetrains in Tidal Current Energy Converters

The enhancement of TCEC power generation capabilities necessitates optimized design of power conversion systems that enable energy capture at reduced cut-in velocities, facilitating the conversion of fluctuating low-speed turbine rotations to stable high-rated outputs. Performance validation of the drivetrain system under varying tidal velocities was accomplished through experimental studies using a TCEC configuration incorporating both hydro-turbine and drivetrain components in controlled flume conditions. Figure 2 illustrates the experimental TCEC configuration, including a hydro-turbine, a gearbox, and a hypoid gear pair. The extractable hydrokinetic power from tidal currents via a hydro-turbine can be expressed as

$$P_r = \frac{1}{2}\rho A_r C_p v_{tidal}^3, \tag{1}$$

where A_r is the hydro-turbine swept area, ρ is the seawater density, C_p is the power coefficient, and v_{tidal} is the tidal current velocity. Equation (1) quantifies the extractable energy for a specified hydro-turbine's swept area operating at a defined power coefficient C_p within a tidal stream. The hydro-turbine's power coefficient C_p primarily correlates with its tip-speed ratio (TSR), which is

$$C_p(\lambda, \beta) = C_Q(\lambda, \beta)\lambda, \tag{2}$$

where $C_Q(\lambda, \beta)$ is the design-dependent torque coefficient and λ is the TSR, which is

$$\lambda = \frac{\omega_t r_t}{v_{tidal}}, \tag{3}$$

with r_t is the rotor radius and ω_t is hydro-turbine's angular velocity. For this study, the hydro-turbine's torque coefficient is [30]

$$C_Q(\lambda, \beta) = 0.5\left(\frac{116}{\gamma} - 0.4\beta - 5\right)e^{-\frac{21}{\lambda}} + 0.0068\lambda, \tag{4}$$

where

$$\frac{1}{\gamma} = \frac{1}{\lambda + 0.08\beta} - \frac{0.035}{\beta^3 + 1}, \tag{5}$$

with β is the pitch angle, i.e., 15° in this study. Using the TSR in Equation (3), hydro-turbine's angular velocity is

$$\omega_r = \frac{\lambda v_{tidal}}{r_t}. \tag{6}$$

The TCEC operational torque, crucial for drivetrain load distribution analysis, can be expressed as

$$T_r = \frac{1}{2}\rho A_r r_t C_Q v_{tidal}^3. \tag{7}$$

This operational torque serves as the primary input parameter for the drivetrain system. The drivetrain facilitates energy transfer from the generated power P_r to the generator assembly. Maintaining optimal performance across variable tidal velocities requires consistent TSR regulation at its designed optimal value.

See ABS Houston, TX Letter Ref WOO671925 dated 14-NOV-2026

Document must be opened with Adobe to view all ABS amendments.

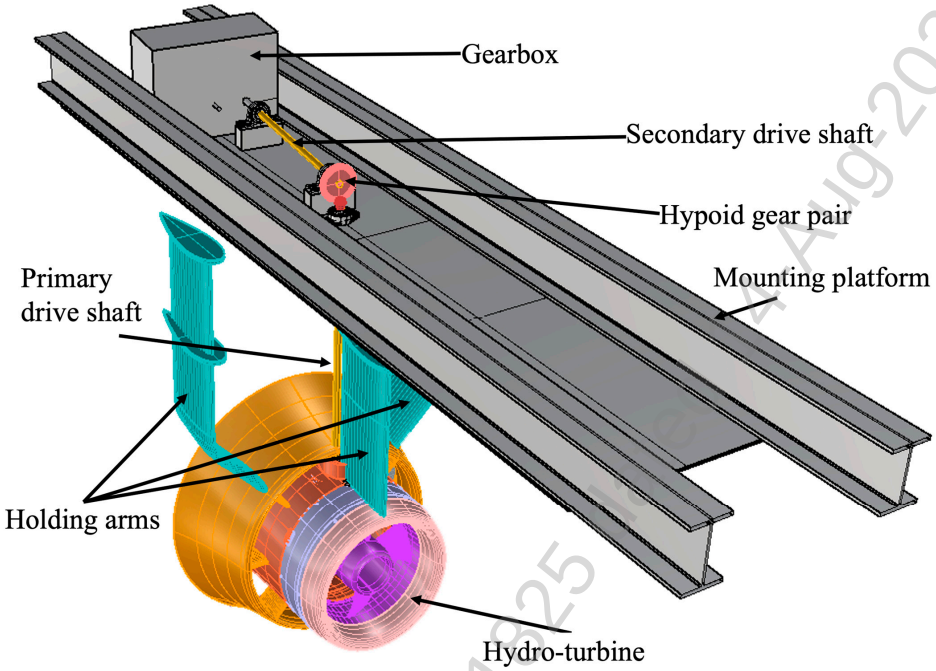

Figure 2. Layout structure of the TCEC, including the hydro-turbine, a hypoid gear pair, and the gearbox [30].

The dynamic torsional model of the hypoid gear under variable tidal current energy-harvesting conditions is shown in Figure 3, and its torsional equations include Equations (8) and (9), which serves to solve the torsional vibrations of the pinion and gear, respectively. This study confines attention to the dynamic behavior under two different tooth contact conditions subject to different milling settings [31]. Thus, TE and MS of two pairs of gears obtained from the respective milling settings are used as parametric input conditions to the torsional equations. The dynamic model excludes the translational vibrations of bearing systems of the rotor system, focusing instead on extensive experimental tests using data from a 3-axis accelerometer.

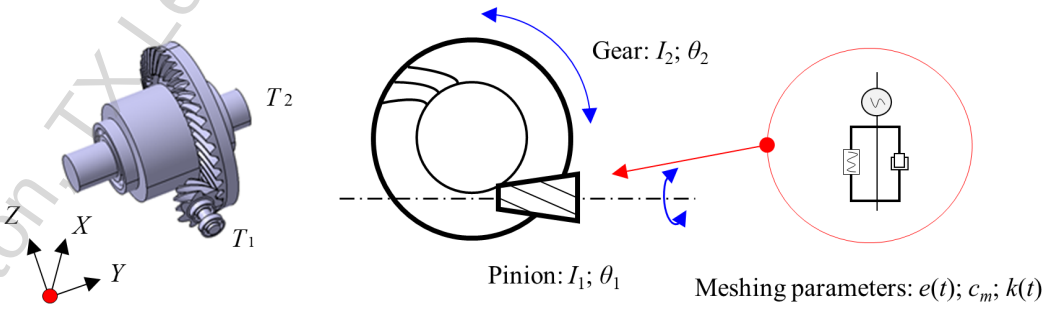

Figure 3. A dynamic model of a hypoid gear system to reflect its angular vibrations.

The torsional equations to solve the torsional vibrations of the pinion and gear are written as

$$I_1\frac{d^2\theta_1}{dt^2} + R_1c_m\left(R_1\frac{d\theta_1}{dt} - R_2\frac{d\theta_2}{dt} - R_1\frac{de(t)}{dt}\right) + R_1k_m(t) = T_r(t), \tag{8}$$

$$I_2\frac{d^2\theta_2}{dt^2} + R_2c_m\left(R_1\frac{d\theta_1}{dt} - R_2\frac{d\theta_2}{dt} - R_2\frac{de(t)}{dt}\right) + R_2k_m(t) = i_hT_r(t), \tag{9}$$

where θ_1 and θ_2 are rotation angles of the pinion and the gear, respectively, R_1 and R_2 are radii of contact points on the pinion and gear, respectively, I_1 and I_2 are the moment of

See ABS Houston TX Letter ref WC0671925 dated 14 Aug 2026

Document must be opened with Adobe to view all ABS amendments.

inertia of the pinion and the gear, respectively, i_h is the gear ratio, c_m, $k_m(t)$, and $e(t)$ are meshing damping, MS, and TE of the hypoid gear rotor system, respectively. Meshing damping c_m, which reflects the effects of viscous and friction, is assumed to be constant in this study. The time-varying MS is an unknown function that can be expressed as $k_m(t) = f(R_1\theta_1 - R_2\theta_2 - e(t))$, which means its value is affected by the combination of angular deviations from the theoretic conjugate position $R_1\theta_1 - R_2\theta_2$ of the contact point on the pinion and the gear tooth surfaces, and the static TE $e(t)$ over meshing cycles.

3. FE Tooth Contact Model Under Variable Tidal Current Conditions

This investigation analyzes the dynamic behavior characteristics of hypoid gear rotor systems under variable tidal current conditions, focusing on the comparative assessment of different tooth contact patterns generated through specialized milling parameters. TE and MS variations for two distinct gear pair configurations are computed using a high-fidelity FE tooth contact model, which incorporates bidirectional loading profiles characteristic of tidal current fluctuations. The precision of the three-dimensional hypoid gear model, particularly critical for the precise computation of TE and MS under reversing tidal flows, is established through an advanced geometric construction methodology that accounts for time-varying contact conditions. This methodology enables a detailed analysis of the behavior of tooth contact during critical tidal flow transition periods, where the loading direction changes significantly impact gear mesh characteristics.

3.1. Tooth Contact Model

This section presents the modeling method of 3D hypoid gears and the FE analysis of the 3D model for the approach in detail to TE and MS. CATIA is well known for the ability of model work to construct complex surfaces, so software is applied to construct the 3D model of hypoid gears. In the simulation of this study, special machines Gleason 116 and 609 are chosen to generate the tooth surface of the specified pair of hypoid gears in CATIA. The face-milled process is applied to machine the pinion and the gear. Basic Visual programming codes drive the milling process through the Macro interface of CATIA, which simulates Gleason 116 generating the pinion and Gleason 609 forming the gear. Figure 4 shows the grinding settings of the Gleason 116 machine tool in Figure 4b and 609 in Figure 4c, respectively, and Figure 4a the grinding process of the pinion and the gear that illustrates the relative positions of the 3D cutter head and the workpiece. The pinion generating settings include ten: four workpiece settings, axial position X_{p1}, horizontal position X_1, vertical position E_{01} and root angle δ_{M1}; four cutter-head settings, S, q, i, and j; and the rolling angle of the workpiece Ψ, and the cradle angle $q = \Psi / m_{1c}$, where m_{1c} is the rolling ratio. Gear formation settings include six: four workpiece positioning settings, i.e., X_2, X_{p2}, E_{02}, and δ_{M2}; and two cutter-head positioning settings, i.e., H and V.

Figure 4a shows that Boolean operations remove the cutter-head solid from the intersection with the workpiece solid at each predetermined workpiece angular position according to the rolling ratio in CATIA's Part Design module. The tooth groove, thereby, is composed of a number of strip surfaces that should be stitched together. In CATIA's Generative Shape Design module, strip surfaces are extracted and joined together, and uniformly distanced partition planes that are vertical to the pinion shaft axis are created. The intersection curves where the generated tooth groove intersects with the partition planes are extracted, and they are replaced by spline curves in CATIA's multi-sectional surface module. An integrated tooth surface is thereby constructed from these spline curve sections in CATIA's Generative Shape Design module. A cover is added to the integrated tooth surface and is sealed together, and in the Part Design module, the sealed tooth surface again becomes a solid tooth through the close-surface operation. Following some other

See ABS Houston, TX Letter ref. 1006718025 dated 14-Aug-2025

Document must be opened with Adobe to view all ABS amendments.

solid editing work, the 3D pair of solid hypoid gears are finally worked out as shown in Figure 5a.

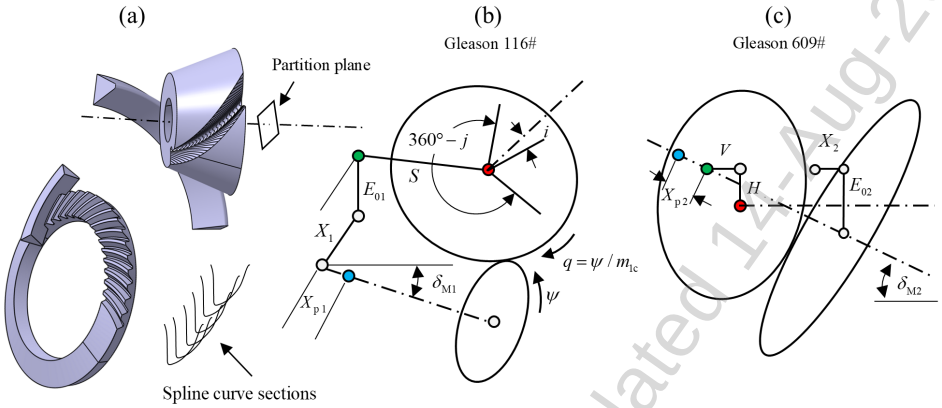

Figure 4. Machining simulations of hypoid gears: (**a**) 3D face-milled process showing relative positions of cutter-head and workpiece of the pinion and the gear, (**b**) generating settings of machine tool for the pinion, and (**c**) forming settings of machine tool for the gear.

Figure 5b shows a piece of the FE model split from the complete hypoid gears in the HYPERMESH version 9.0 software. This study only requires a six-tooth pinion and gear for analysis, which significantly saves computing time and provides sufficient accuracy. The incompatible mode of element C3D8I is configured in HYPERMESH to perform grid division of the FE model, which is good at a high resolution of contact stress. Details of the six-tooth FE model of hypoid gears include that the pair has a total of 308,988 elements with 350,998 nodes, mesh density is 25 × 62 nodes for the master tooth surface (drive side of the pinion), and 32 × 72 nodes for slave tooth surface (driven side of the gear). The element density of the surface of the slave tooth is predefined higher than the surface of the master tooth at 149% to avoid any penetration into each other. However, the same density would give more accurate results. Physical parameters include material characteristics: Young's modulus and Poisson's ratio predetermined as $E = 2.1 \times 108$ N/mm^2, and $v = 0.3$ in this study. TE and MS simulations were managed by ABAQUS. To promote convergence, a small approach angle of 0.001 is set as an initial angle, which is an effective measure to ensure that the pinion and gear teeth are in slight contact.

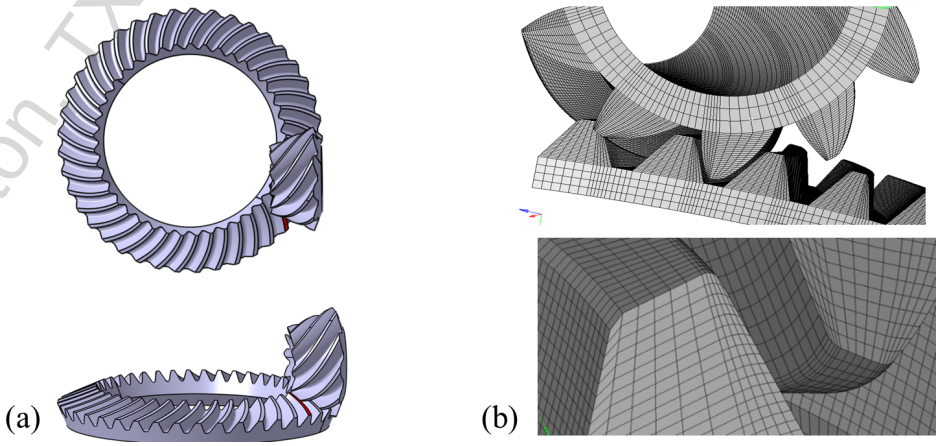

Figure 5. 3D modeling of the hypoid gear pair: (**a**) 3D model of the hypoid gear pair in CATIA, and (**b**) its FE tooth contact model using HYPERMESH.

3.2. TE and MS of the Hypoid Gear Pair

TE of gears, including the unloaded UTE and the loaded LTE, is commonly defined as the angular difference of the actual angular position of the driven gear from

See ABS Houston_TX Letter ref WCC/18255 dated 14-Aug-2025

Document must be opened with Adobe to view all ABS amendments.

its mathematical conjugate angular position. Therefore, TE is conceptually expressed as $e(\varphi_1) = \varphi_2 - (z_2/z_1)\varphi_1$, where z_1, z_2, φ_1, φ_2 denote the tooth number and the actual angular positions of the pinion and gear, respectively. TE of hypoid gears is caused by multiple factors, such as geometric tooth-form deviation and assembly error under unloaded conditions and loaded conditions. TE also involves surface compression, bending and shear, and torsion of the pinion and the gear and its shaft systems. For hypoid gears, the geometric tooth-form deviation relates to its generating method, and the theoretic conjugate point only exists at the reference point on the center of the pinion and the gear tooth surfaces, which is the biggest difference from the involute gears. Missing the mathematic reference tooth surface makes it extremely difficult to obtain an accurate TE of hypoid gears by either the analytic or the numeric method; in contrast, involute gears have a reference datum involute surface. The FE method that relies on computing power is increasingly becoming an effective tool to produce a relatively accurate TE with the development of computing technology. However, TE by the FE method is still dependent on the accuracy of the tooth contact model to simulate the generating process of actual milling machines. The detailed construction process of 3D and FE models of hypoid gears, which serve to compute TE and MS of this section, are presented in Section 3.1.

In addition to TE, the FE method is also wildly involved in the MS calculation of involute gears. Cooley [13] proposed two determining approaches of the average slope and the local slope to calculate the MS of the spur gears using the FE method. In Cooley's two approaches, the FE tooth contact model of spur gears is utilized for obtaining tooth contact compression, tooth bending and shear for a span of specified torque loads. Cooley made careful comparisons between the two approaches and came up with suggestions that the average slope more resembles a static analysis and that the local slope can work well on dynamics. The average slope mathematically is an arithmetic formula, and the local slope is a finite-difference formula. The local slope approach is applied to calculate the time-varying MS for hypoid gears supported by the data from the FE tooth contact model.

Stiffness refers to the ability of a material or structure to resist elastic deformation subject to force. The composite elastic deformation of a geared system should include many components, such as Hertz tooth contact compression, tooth bending and shear, shaft system torsions, etc. Thereby, the composite static mesh stiffness of a geared rotor system at an instant time can be expressed as

$$\frac{1}{k_m} = \frac{1}{k_c} + \frac{1}{k_b} + \frac{1}{k_s} + \frac{1}{k_t}, \tag{10}$$

where k_m is the composite mesh stiffness, k_c, k_b, and k_s are the separated stiffness caused by the tooth contact compression, tooth bending, and shear, respectively, K_t is the local stiffness of the mesh caused by shaft torsions as it transmits the torque. Typically, a hyoid gear pair has multiple teeth in contact simultaneously. Chang [32] thought that the mesh stiffness of multi-tooth contact is something like a set of parallel contact springs and suggested that the global composite stiffness of gears is expressed by summing up all discrete contact points to cover all major contact lines, giving

$$K_m = \sum_{i=1}^{N} k_m^{(i)}, \tag{11}$$

where N is the amount total of discrete segments, and k_m is the mesh stiffness of the mth tooth pair in contact. The finite-difference stiffness formula of the local slope approach for the mth single tooth pair in contact is represented as

See ABS Houston, TX Letter ref 1006719825 dated 14-AUG-2025

Document must be opened with Adobe to view all ABS amendments.

$$k_m = \frac{F_n(q_n + \Delta q_n) - F_n(q_n - \Delta q_n)}{2\Delta q_n}, \tag{12}$$

where F_n is tooth contact force, q_n is composite mesh deflection of single tooth contact corresponds to the total approaching distance of a tooth contact segment caused by tooth contact compression, tooth bending, and shear, and Δq_n is a specified small increment of mesh deflection, i.e., finite-difference term. Equation (12) can also be rewritten as

$$k_m^{-1} = \frac{q_n(F_n + \Delta F_n) - q_n(F_n - \Delta F_n)}{2\Delta F_n}. \tag{13}$$

It is much more convenient to give a desired incremental size of ΔT, and correspondingly it yields ΔF_n. It should be noted that excellent convergence is reported by setting the increment size at 1% of the nominal torque load [13]. This approach may cover all interesting torque ranges and avoid possible multiple stiffness curves due to the nonlinearity of contact deformation.

4. Experimental Testing and Data Process

4.1. Experimental Setup

A bevel gear testing rig in Figure 6 integrates high-precision rotary encoders for measuring torsional vibrations and a triaxial accelerometer for capturing translational responses under simulated turbine speed profiles ranging from 50 to 1400 rpm and torque loads up to 450 Nm. Measurement facilities in the testing rig maintain sampling frequencies at four times the mesh frequency to ensure adequate resolution of second-order primary resonances during flow transitions, enabling comprehensive characterization of dynamic behaviors across both rotational and spatial domains. Measurement facilities of the testing rig include (1) a magnetic brake, (2) a hypoid gear pair, (3) rotary encoders, (4) torque sensors, (5) a motor, and (6) a PCB Piezotronics 3-axis accelerometer. LTE is produced using measured data on the angular positions on the pinion and gear sides according to its definition formula in Section 3.2. LTE is obtained when the rotor system runs under quasistatic conditions for a certain number of angles at a very low speed. Translational vibrations in the x, y, and z-axis directions are measured by the 3-axis accelerometer on the upper surface of the hypoid gearbox.

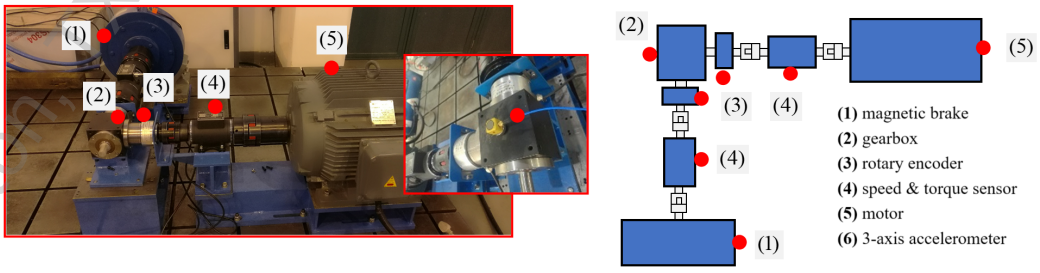

Figure 6. Bevel gear pair testing rig to measure torsional and translational vibrations by rotary encoders and a 3-axis accelerometer, respectively.

The measurable finest angle of the optical rotary encoders on the input side is $2\pi/2^{17}$ rad, and the output side is $2\pi/2^{21}$ rad. Such resolution ratios on both sides can ensure the desired precision for the research objective of this study. The details of the acceleration meter are as follows: A PCB Piezotronics 3-axis accelerometer to measure translational vibrations in the x, y, and z directions, type 356B18, and a National Instruments NI-9234 data acquisition board that connects to the sensor to collect vibration data in three directions. Key performances are: sensitivity ± 10% of 102 mV/(m/s^2); measurable

See ABS Houston, TX Letter WC 16-1825 dated 14-Aug-2026

Document must be opened with Adobe to view all ABS amendments.

frequency range 0.5–3000 Hz with ±5% sensitivity and bandwidth 110,000 Hz. Data of x, y, and z vibrations are processed by ORIGIN to analyze frequency components and by MATLAB R2024b for comprehensive analysis and reprocessing. The mesh frequency is calculated by $f_m = n$ rpm $\times$ N_1 / 60 s, where n rpm is the speed of input on the pinion side, and the sampling frequency must meet $f_s > 2 - 5f_m$ according to the sampling theory.

The investigation requires a large number of tests so that the steady-state data are collected by continuously increasing the load and speed within the respective ranges in Section 5.3. The particular concern is that the investigation avoids directly comparing torsional vibrations of the rotor system of the test rig with simulations. Torsional motion equations in Equations (8) and (9) cannot analyze real-world conditions that neglect certain factors such as manufacturing errors, friction, material nonlinearity, and temperature variations. The direct comparison between experiment and simulation is likely to become endless discussions about the accuracy of tests and how factors are considered in simulation. The response of loads and speeds in the frequency domain is a desirable method to eliminate the high-frequency components of exciting sources caused by most manufacturing errors.

4.2. Data Process

The data collected from experimental tests are not suitable for direct comparison with simulations, which means that the data have to be processed in a certain form before being compared to the simulations. It is extremely difficult to capture the transient state to compare simulations and experiments under dynamic conditions of the rotor system of hypoid gears at a certain instant time of interest in practice. However, it is more practical to compare the load response and the speed response in the steady state, which reflects typical dynamic behaviors of hypoid gears but can also be easily compared between simulations and experiments. The comparison is conducted mainly in the frequency domain and in the form of average maximum magnitude (AMM) and root mean square (RMS) in a steady state after a specified period of time. The time-domain data of vibrations picked from simulations and experiments are processed into the form of AMM and RMS before they are compared to each other. The load and speed responses are used to evaluate the dynamic behaviors of hypoid gear rotor systems under different tooth contact conditions. Detailed comparisons are performed next in Section 5 for hypoid gears of a domestic popular vehicle. The design data and generating settings are listed in Table 1.

Table 1. Basic design specifications of the hypoid gear pair 41 $\times$ 11 on the driving side.

Design Parameters	Symbols	Pinion	Gear
Number of teeth	z_1, z_2	11	41
Spiral direction		Left	Right
Pitch diameter	d_2	N/A	295.00
Shaft offset (mm)	E		25.40
Face width (mm)	b_1, b_2	44.57	41.00
Outer cone diameter (mm)	d_{e1}, d_{e2}	156.32	273.57
Mean spiral angle (deg)	β_{01}, β_{02}	45.08	48.08
Pitch cone angle (deg)	δ_1, δ_2	11.82	77.92
Face cone angle (deg)	δ_{a1}, δ_{a2}	16.18	78.57
Root cone angle (deg)	δ_{f1}, δ_{f2}	11.17	73.45
Face cone point	O_{a1}, O_{a2}	−0.68	0.64
Pitch cone point	O_{H1}, O_{H2}	−7.24	0.39
Root cone point	O_{f1}, O_{f2}	−1.62	0.08

For torsional vibrations, the angular positions in the unit of μrad of the pinion and the gear are measured by two rotary encoders on both shafts. Respective torsional vibrations of the pinion and the gear are combined as DTE when the rotor system of

See ABS Houston TX Letter ref:(0067825 dated 11-AUG-2026

Document must be opened with Adobe to view all ABS amendments.

the hypoid gears runs at high speed, and the dynamic effect must be considered. Let $\Delta\varphi(\tau)|_k = [\Delta\varphi_1, \Delta\varphi_2, \Delta\varphi_3, \Delta\varphi_4, \ldots, \Delta\varphi_n]$ denote the n number of dynamic LTEs collected from its theoretic formula $\Delta\varphi = \varphi_o - \gamma\varphi_I$ in steady state for a specified period, where τ is the specified period of the measurement operation, $\Delta\phi_n$ is the error value for a predefined time interval by dividing τ, and k is one of the tests or measurement operations, i.e., different k corresponds to any of the load and speed differences of the numbers of test operations. For each test operation k under different load and speed conditions, q_a denotes the AAM operation obtained from $q_a = maxium(\Delta\varphi_n)|_k$, and q_{rms} denotes the RMS operation obtained from $q_{rms} = [\sum(\Delta\varphi_n|_k)/n]^{0.5}$.

For translational vibrations, let $X|_k = [x_1, x_2, x_3, \ldots, x_n]$, $Y|_k = [y_1, y_2, y_3, \ldots, y_n]$, and $Z|_k = [z_1, z_2, z_3, \ldots, z_n]$ denote the collected vibration data in x, y and z-axis directions, respectively, where k is the kth test operation under different load and speed conditions $[T, \omega_p]|_k$. The collected time-domain vibration data $[x_t, y_t, z_t]|_k$ in an instant of time t of experiments is transformed into frequency domain vibration data $[x_f, y_f, z_f]|_k$ in the Origin software by performing the fast Fourier transform (FFT). Let n, ω_p, f_r, and f_m denote the order number, the pinion speed, the revolution, and the mesh frequencies of the rotor system, respectively. Thus, the revolution frequency is $f_r = 60\omega_p$, the mesh frequency is $f_m = z_1 f_r$, and the frequency of the primary resonances at the nth order (n = 1, 2, 3, ...) is $f_n = nz_1 f_r = 60nz_1\omega_p$. The RMS operation that expresses the overall intensity of the vibration is $d_{rms} = [\sum(x_{fn}^2 + y_{fn}^2 + z_{fn}^2)/3)]^{0.5}|_k$ obtained from vibrational magnitudes of the frequency domain of $[x_{fn}, y_{fn}, z_{fn}]|_k$ in x, y and z directions at frequencies f_n of different orders n.

5. Results and Discussion

This study uses two hypoid gear pairs for experimental testing, with the gear and pinion produced by Gleason 116 and 609 machine tools, respectively. Design specifications for hypoid gear pairs are listed in Table 1.

The pinion speed is set to different test conditions for testing variation effects in tidal current and flow reversals. For this study, the hypoid gear model 41 × 11 is subject to two different machine-tool settings to produce two pairs of gears under two different tooth contact conditions according to the machine-tool settings in Tables 2 and 3, respectively. One hypoid gear pair has a normal tooth contact condition, and the other has a slight edge contact condition to generate a different LTE and MS. Two hypoid gear pairs are obtained in two different tooth contact conditions by modifying the cutter radius and the other machine-tool settings, the details of which are omitted here.

Table 2. Machine-tool settings of gear pair No. 1 in the normal tooth contact condition.

Settings of Machine Tool	Symbols	Pinion	Gear
Sliding base	X_1, X_2	28.78	87.94
Machine center to back	X_{p1}, X_{p2}	2.63	−3.63
Flank offset	E_{01}, E_{02}	24.38	76.59
Machine root angle (deg)	δ_{M1}, δ_{M2}	357.78	20.40
Cradle radius	$S; V, H$	117.12	25.38, 99.50
Cutter-head title angle (deg)	i	18.59	0
Cutter-head swivel angle (deg)	j	−43.53	0
Cutter-head diameter	$2r_{c1}, 2r_{c2}$	229.36	112.95
Cutter-head blade angle (deg)	α_{01}, α_{02}	14	20
Roll ratio	m_{1c}, m_{1c}	3.67	0
Milling method		generating	forming

See ABS Houston, TX Letter ref WOC 21825 dated 14 AUG 2025

Document must be opened with Adobe to view all ABS amendments.

Table 3. Machine-tool settings of gear pair No. 2 in the tooth edge contact condition.

Settings of Machine Tool	Symbols	Pinion	Gear
Sliding base	X_1, X_2	23.57	87.94
Machine center to back	X_{p1}, X_{p2}	−0.86	−3.63
Flank offset	E_{01}, E_{02}	22.39	76.59
Machine root angle (deg)	δ_{M1}, δ_{M2}	358.35	20.40
Cradle radius	$S; V, H$	115.68	25.38, 99.50
Cutter-head title angle (deg)	i	17.95	0
Cutter-head swivel angle (deg)	j	−40.67	0
Cutter-head diameter	$2r_{c1}, 2r_{c2}$	245.45	112.95
Cutter-head blade angle (deg)	α_{01}, α_{02}	14	20
Roll ratio	m_{1c}, m_{1c}	3.63	0
Milling method		generating	forming

5.1. LTE and Its Harmonic Components

LTEs are obtained from the simulation and the experiments under a torque load of 50 to 450 Nm, respectively, under quasistatic conditions. The speed is fixed at a very low 50 rpm, at which the dynamic effect can be neglected. In an ABAQUS-based FE analysis, the angular positions of the pinion and the gear can be read, respectively, at each step of mutual rotations from pre-setting in the software. In experimental tests, the angular positions of the pinon and the gear can be collected from rotary encoders. LTEs are therefore calculated according to its definition formula in Section 3.2. The two pairs of solid gears of the hypoid gears are produced by Gleason 116 and 609 milling machines, and two 3D tooth contact models for FE analysis are constructed in CATIA according to the generating methods in Section 3, based on the model data in Table 1 and two different settings of the machine tool in Tables 2 and 3, respectively. Then, two 3D models are transformed into FE tooth contact models by completing the mesh division. The tooth contact analysis for two different FE models is performed in ABAQUS, and experimental tests for two solid gear pairs are conducted on the test rig of Figure 6. Figures 7–9 show their respective contact patterns, LTE, and their harmonic components of the primary resonances in the frequency domain under two different contact conditions of the teeth of interest when the pinion shaft has exerted a torque of 350 Nm. Under normal tooth contact conditions, LTE curves from both the FE model and experiments have a regular sine shape, whereas, under edge tooth contact conditions, they do not. The fast Fourier transformation (FFT) is performed for the LTE data in the time domain of the simulation and experiment, and Figure 9 shows their respective harmonic components of the primary resonances from frequencies $1f_m$ to $8f_m$, where f_m is the mesh frequency. The simulation result is similar to the experiment, which suggests that hypoid gears under edge tooth contact conditions have more harmonic components than under normal tooth contact conditions. Experimental results suggest that in the frequency domain, LTE has a lot of high-frequency harmonic components under both edge and normal tooth contact conditions. In addition, tooth contact patterns demonstrate high sensitivity to milling parameter variations under bidirectional tidal loading conditions, resulting in distinct TE and MS characteristics during flow reversals.

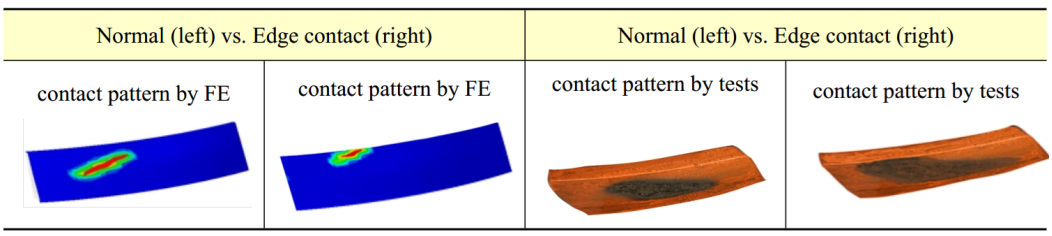

Figure 7. Contact pattern comparisons between two gear pairs under different tooth contact conditions.

See ABS Houston, TX Letter ref: WQ067835 dated 14-Aug-2026

Document must be opened with Adobe to view all ABS amendments.

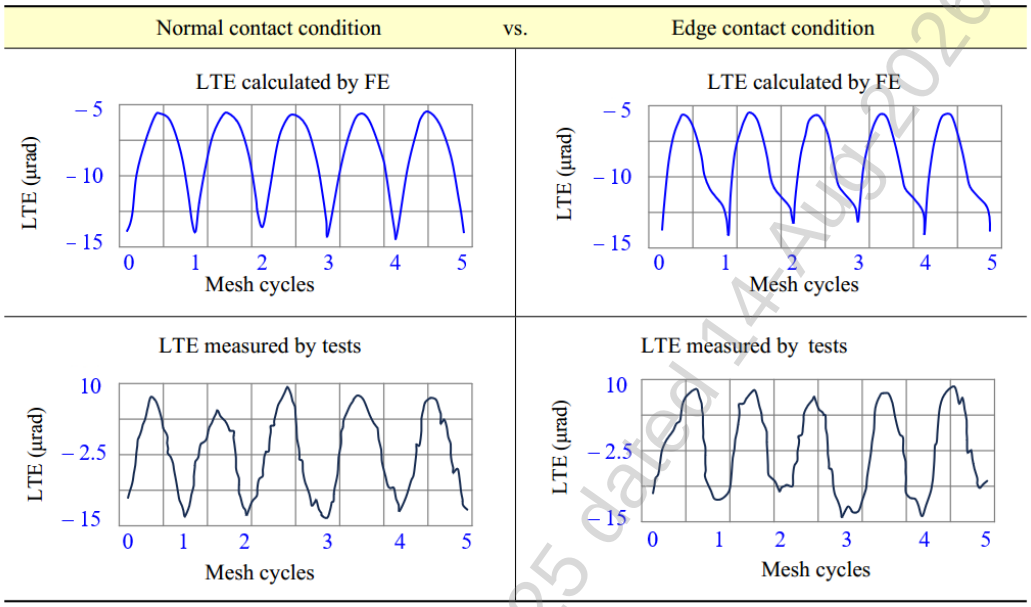

Figure 8. LTE yielded from the FE method and rolling tests under input torque 350 Nm in two different contact conditions.

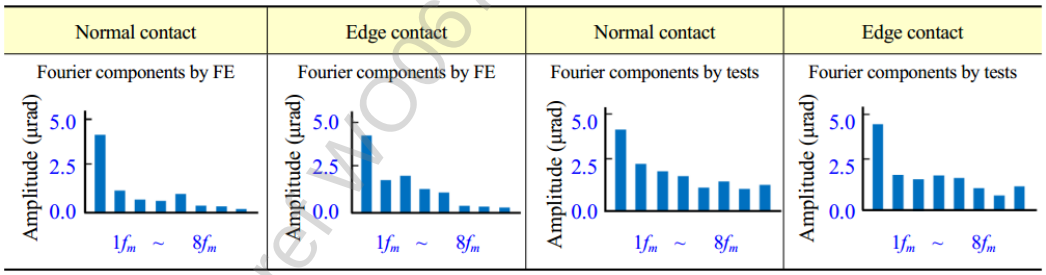

Figure 9. Fourier components of LTE under different contact conditions.

LTE, as one of the primary exciting sources, contributes to the unique dynamic characteristics of hypoid gears, and loaded TE is often used to predict possible dynamic behaviors of the rotor system. However, the exact dynamic behaviors of the hypoid gear rotor system have to be evaluated by torsional vibrations; in most cases, it is reflected by the dynamic TE in the form.

Primary resonances of the first five orders of the Fourier series of LTE $e(t)$ thus can be written as

$$e(t) = e_0 + \sum_{i=1}^{5} e_i \cos(i\omega_h t + \phi_i) \tag{14}$$

where i and ω_h are harmonic order and mesh frequency, respectively, e_0 and e_i are the fundamental and the ith order harmonic component of LTE, respectively, and ϕ_i is phase position.

5.2. MS and Its Harmonic Components

MS is extremely difficult to measure directly from rotary encoders in experimental tests, according to the accessible public literature. In this study, MS under two different tooth contact conditions is obtained from the Cooley local slope approach using the finite-difference formula presented in Section 3.2, based on the angular position data of the FE tooth contact model.

Figure 10 shows the MS of two pairs of gears of the chosen commercial hypoid gears model, which are obtained from the finite-difference formula of Cooley's local slope approach under two different normal and edge tooth contact conditions in the simulations

See ABS Houston, TX Letter ref WQ0671825 dated 14 Aug 2026

Document must be opened with Adobe to view all ABS amendments.

using data from the FE tooth contact analysis. The MS of the gears is usually shaped like the letter "n", i.e., there are steep rises and falls on two sides, suggesting that the contact shift occurs on different teeth. The Fourier series of MS yielded from FFT replaces time-domain MS as input nonlinear exciting source to perform dynamic analysis using the dynamic motion model presented in Section 2, which provides a direct correlation between the exciting and response frequencies for this study. The time-varying MS $k_m(t)$ for primary five orders of Fourier series shown in Figure 11 thus can be written as

$$k(t) = k_0 + \sum_{j=1}^{5} k_j \cos(j\omega_h t + \varphi_j), \tag{15}$$

where j and ω_h are harmonic orders and mesh frequency, respectively, k_0 and k_j are the fundamental and the jth order harmonic components, respectively, and φ_j is phase position of the jth harmonic component. In parametric theory, the time-varying MS of the gear pair may enhance the second-order harmonic vibration of its rotor system.

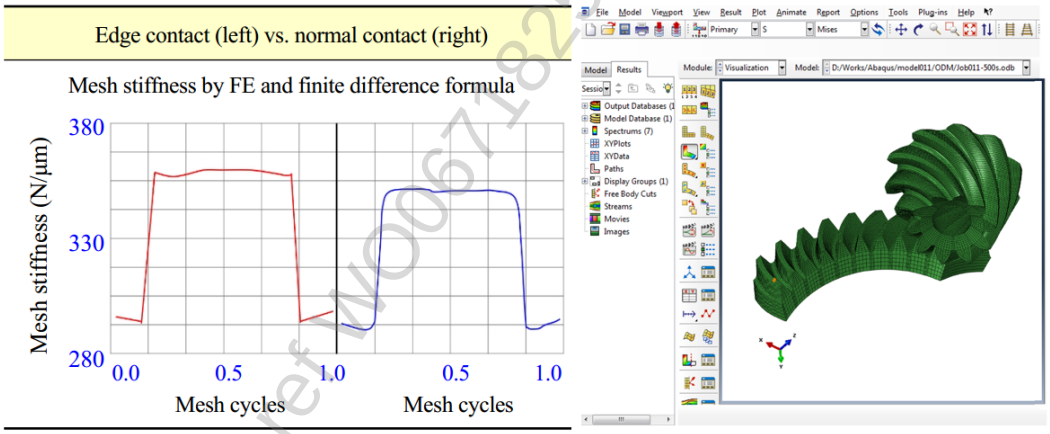

Figure 10. MS simulation results under two different tooth contact conditions and its Abaqus analysis image.

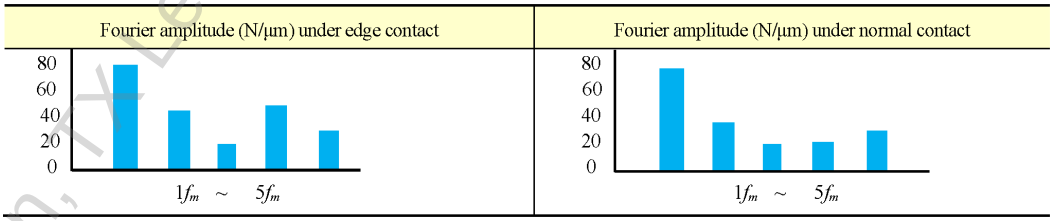

Figure 11. Harmonic components of MS under two different tooth contact conditions.

5.3. Torsional Vibrations

The torsional vibrations of the pinion θ_1 and the gear θ_2 are usually illustrated by DTE (θ_1, θ_2) which graphically assesses the dynamic characteristics of the geared systems. Figure 12 compares two DTEs in steady state under two different tooth contact conditions of normal and edge, and the results of two tooth contact conditions are obtained from Equations (8) and (9). The DTE figures suggest that the periodicity in the case of normal tooth contact is better than in the case of edge tooth contact, or in the case of edge tooth contact, the rotor system may behave periodically for a sufficiently long period. Comparisons also suggest that the dynamic behavior of hypoid gears under the edge tooth contact condition has more complex harmonic components. In contrast, LTEs under two different tooth contact conditions in a quasistatic state have perfect periodicity due to the milling consistency in each tooth-form geometric deviation shown in Figure 8.

See ABS Houston, TX Letter Ref WQ067825 dated 14-Aug-2025

Document must be opened with Adobe to view all ABS amendments.

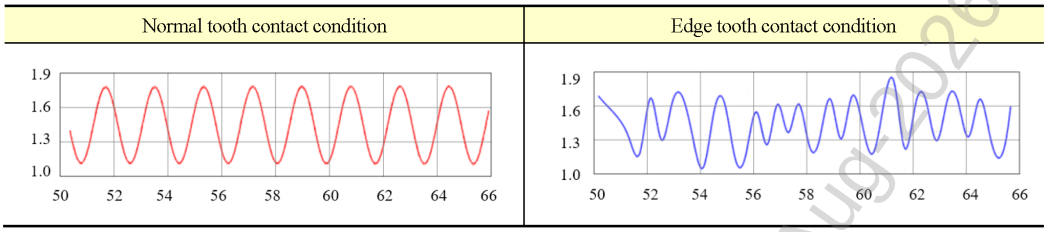

Figure 12. Dimensionless dynamic TE under two different tooth contact conditions of normal and edge in steady state.

It is difficult to compare DTEs directly between simulations and experiments, which are yielded, respectively, from the torsional equations and data of rotary encoders as measured. In reality, torsional vibrations of experiments are resultant signals that may include various harmonic components such as shaft revolution and noise of bearing systems, in addition to mesh frequency and harmonic frequencies excited by TE and MS. The DTEs of experimental results are filtered to eliminate the shaft revolution signal in low frequency and the noise signal of bearing systems in high frequency before compared to that of simulations. Comparisons of load and speed responses are performed between the filtered experimental data and the simulation data, which are evaluated by AMM and RMS under two different tooth contact conditions. The proposed comparisons of the load and speed responses in AMM and RMS are expected to provide a comprehensive and accurate understanding of the dynamic characteristics of the gear systems. In simulations, the torsional vibrations of the pinion θ_1 and the gear θ_2 are solved numerically using the Runge–Kutta method in Equations (8) and (9), which adopts c_m, $e(t)$, and $k(t)$ to be used as equation parameters to investigate the response of load and speed to exciting sources of TE and MS. The mesh damping is a constant c_m = 500 N·s/m. In experiments, the torsional vibrations of the gear pair are measured by two rotary encoders under different experimental testing conditions: the speed ranges from 50 to 1400 rpm on the pinion side, giving a mesh frequency f_m = 0.55–15.4 kHz; and the sampling frequency f_s is set four times the mesh frequency f_m in each sufficiently high test; and the load ranges from 50 to 450 Nm.

AMM and RMS of the load and speed responses are computed according to the data process method presented in Section 4.2, and they are compared between simulations and experiments. Two gear pairs of the normal and the edge tooth contacts are tested under the aforementioned conditions in the previous paragraph, and the measurement procedure starts after the rotor system runs for a long period, which ensures the system has been in a steady state. The blue and red curves in Figure 13 are experimental data in units of 10^{-2} μrad in the left ordinate and simulation data scaled by dimensionless coordinates in the right ordinate, respectively.

Figure 13a,b are load responses (LRs) in AMM and RMS of simulations and experiments, which are observed roughly the same between two different tooth contact conditions of the edge denoted by the dotted line and the normal denoted by the solid line. The load responses in AMM and RMS decrease slightly during light load and then increase continuously, and experiments suggest that the rotor system of hypoid gears is in an unstable state in which behaviors sustained angular vibrations between 50 and 75 Nm of the light input load condition.

Figure 13c–f are the speed response (SR) in AMM and RMS to the pinion speed between simulations and experiments under two different tooth contact conditions of the normal and the edge. Primary resonance vibrations are observed from both simulations and experiments, which are put together in figures. According to Section 4.2, primary resonances at the nth order are $f_n = 60nz_1\omega_p$. Experimental tests of the two pairs of hypoid

See ABS Houston TX Letter Ref WDC071625 dated 14-Aug-2026

Document must be opened with Adobe to view all ABS amendments.

gears suggest that primary resonances of first and second orders occur at f_1 = 858 kHz and f_2 = 1716 kHz, which correspond to pinion speeds of 1300 rpm and 2800 rpm, respectively. Figure 13c–f show that simulations and experiments share similar dynamic behaviors in SRs evaluated by AMM and RMS. Importantly, SR figures show that the gear pair under edge tooth contact condition has a larger magnitude of AMM and RMS during flow reversals according to experiments and simulations, and edge tooth contact has more complex harmonic components, which confirms empirical predictions.

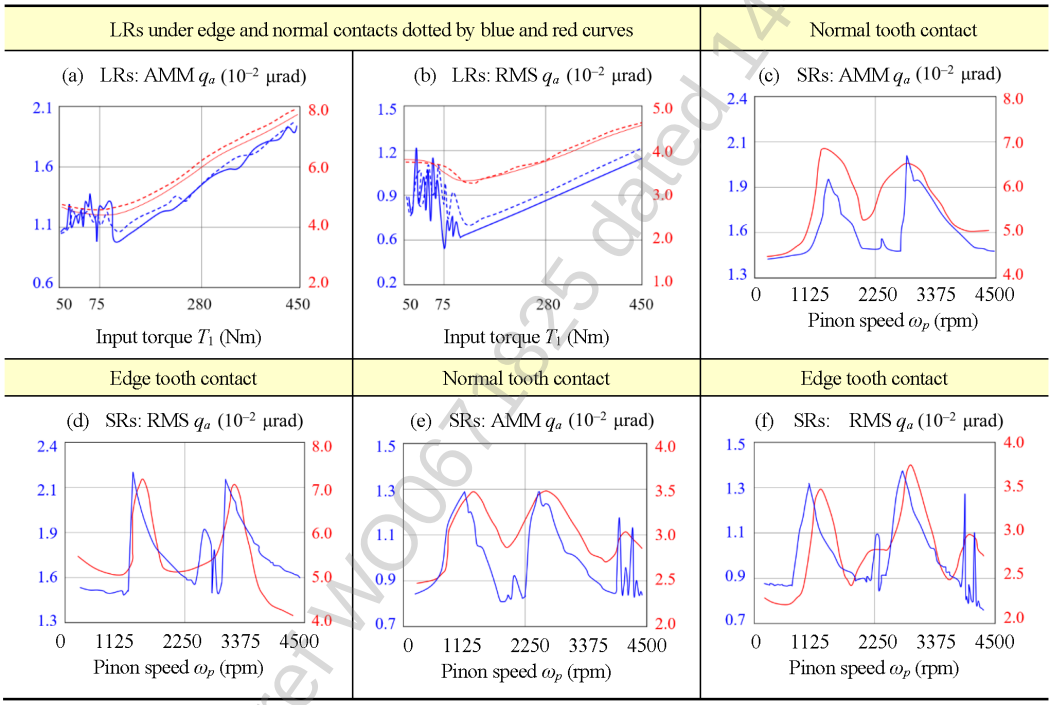

Figure 13. Angular LRs and SRs between experiments and simulations denoted by blue and red curves, respectively.

5.4. Translational Vibrations

Translational vibrations of two pairs of hypoid gears are also investigated by experiments that use an accelerometer shown in Figure 6 to collect vibrational accelerations $[x_t, y_t, z_t]$ of the time domain in x, y, and z directions. The data in the time domain are transformed by FFT into the data in the frequency domain $[x_f, y_f, z_f]$ and then processed into d_{rms}, which reflects the overall intensity of the vibration. The overall intensity of vibrations is for further analysis of gear pairs, and the detailed data process is presented in Section 4.2. Figure 14 shows the vibrational accelerations collected $[x_t, y_t, z_t]$ of the time domain from one of multiple experimental tests under different load and speed conditions. The time-domain vibrational accelerations suggest that z_t in the up and down direction has a slightly smaller magnitude than in the horizontal directions x_t and y_t. Figure 15 shows the vibrations in the frequency domain to examine consistency in different directions x, y, and z under the condition that the pinion speed remains at 3000 rpm. At the remaining speed, frequencies of the first three orders of primary resonances are 1980 kHz, 3960 kHz, and 5940 kHz, respectively. The multiple experimental tests suggest that the magnitudes of primary resonances of the gear pairs of hypoid gears in different directions are different.

The general intensity of vibration d_{rms} that goes with the increase of the pinion speed ω_p is obtained from the accelerations in the collected time domain at each increase in the pinion speed, which corresponds to the nth order vibrational frequency $f_n = 60nz_1\omega_p$. The vibration order n in the gear vibration refers to a dimensionless quantity that represents the frequency of vibration normalized by the rotational speed of a reference component,

See ABS Houston, TX Letter ref WOO61835 dated 14-Aug-2026

Document must be opened with Adobe to view all ABS amendments.

e.g., the gear shaft. It defines how many times a vibration event occurs per revolution of the component. For example, in the first order $n = 1$, vibration corresponds to a frequency equal to the rotational frequency of the shaft, and the order n typically relates to the gear meshing frequency multiplied by n times the shaft speed generated by periodic tooth engagement. The overall intensity of vibration d_{rms} in the frequency domain is compared between two pairs of gears under two different tooth contact conditions by a large number of experimental tests, as shown in Figure 16. The proposed comparisons suggest that the gear pair in the case of edge tooth contact has higher vibrational intensity d_{rms} than in the case of normal tooth contact. The general increase in the intensity of the vibration d_{rms} is significantly correlated with the increase in the pinion speed of the order $n = 2$, which means that the second order of the pair of gears of the hypoid gears increases the power losses in the conversion of the tidal energy. According to the figures, two pairs of gears under different tooth contact conditions of normal in solid line and edge in dashed line share a similar trend in three all orders $n = 1$, 2, and 3. However, the overall vibration intensity d_{rms} in the case of the edge tooth contact increases higher than in the case of the normal tooth contact, along with the rotation speed of order $n = 2$.

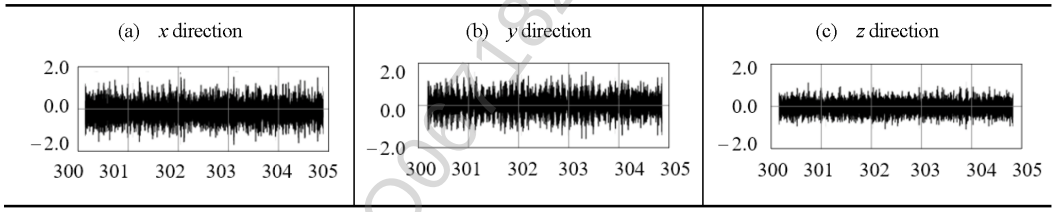

Figure 14. Measured accelerations in unit of g in x, y and z directions for 5 s at pinion speed 3000 rpm.

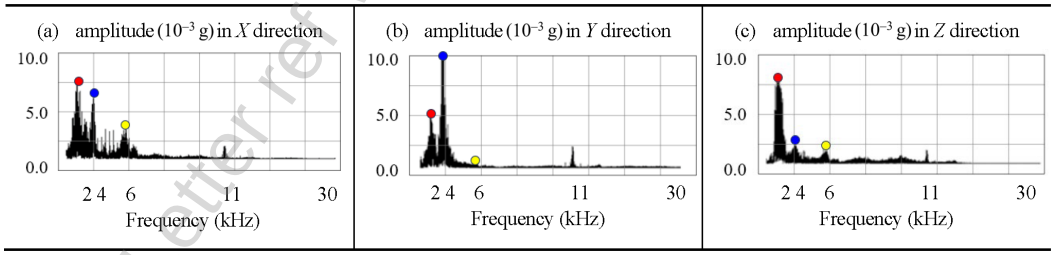

Figure 15. Primary resonances of the first three orders at 1980 kHz, 3960 kHz, and 5940 kHz in x, y, and z directions.

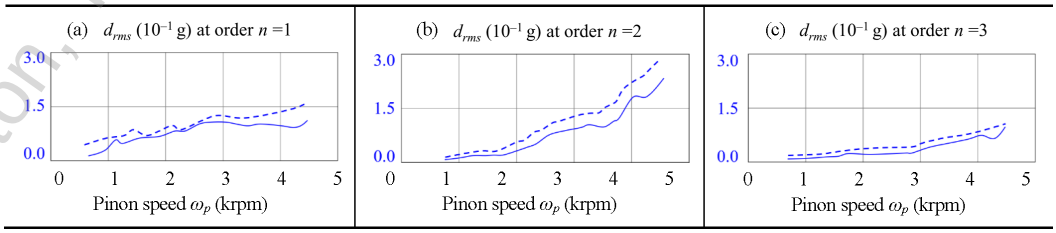

Figure 16. Translational SRs in RMS at orders of $n = 1, 2, 3$, and vibrational frequencies $f_n = 60\,nz_1\omega_p$.

Based on experimental findings and numerical analyses, several key solutions can be proposed for optimizing hypoid gear transmissions in tidal energy-harvesting systems, including: (1) implementation of modified tooth profile parameters during the manufacturing process, specifically adjusting the cutter radius and machine-tool settings to achieve optimal contact patterns that can better accommodate bidirectional loading; (2) development of specialized inspection protocols that focus on characterizing tooth contact patterns under simulated tidal loading conditions prior to deployment, particularly examining behavior during flow-reversal phases where edge contact is most prevalent; and (3) integra-

See ABS Houston, TX Letter ref WOU71825 dated 14 Aug 2026

Document must be opened with Adobe to view all ABS amendments.

tion of advanced monitoring systems utilizing high-precision rotary encoders and triaxial accelerometers to detect early signs of adverse contact patterns, especially monitoring second-order primary resonances, which this study identified as key indicators of edge contact development.

6. Conclusions

This study presents a comprehensive investigation of the dynamic behaviors of hypoid gears under variable tidal current energy-harvesting conditions, with particular emphasis on the effects of tooth contact patterns during bidirectional loading cycles. The study focuses on dynamic responses induced by internal excitation sources, specifically TE and MS, under characteristic tidal current variations and flow reversals. Comparison of torsional and translational vibrations between the two gear configurations, supported by both numerical simulations and experimental validation, yields the following significant findings.

(1) tooth contact patterns demonstrate high sensitivity to milling parameter variations under bidirectional tidal loading conditions, resulting in distinct TE and MS characteristics during flow reversals.

(2) Frequency domain analysis reveals that marginal edge tooth contact significantly amplifies the high-frequency harmonic components of TE and MS, particularly during tidal flow transition periods.

(3) Speed response measurements in multiple experimental trials confirm that edge contact-induced harmonic components generate additional angular vibrations in the high-frequency domain during flow reversals, validating the numerical predictions from the torsional model.

(4) Under variable tidal current conditions, tooth contact patterns significantly influence the dynamics of the system, with second-order primary resonances that exhibit elevated vibration intensities during flow transitions, leading to increased power losses in the conversion of tidal energy.

Generally, edge contact deteriorates the dynamic performance of hypoid gears, adding vibrations to the rotor system, particularly in high-frequency components. The short contact pattern decreases the contact load capacity, and the long contact pattern increases the risk of edge contact according to the tooth contact analysis and the pattern check obtained from the FE analysis and experimental rolling tests. The radius of the cutter head, along with the other generating settings of the pinion, significantly changes the contact length so that the appropriate radius of the cutter head is important, and the recommended cutter head for the pinion of the 41×11 hypoid gear pair is the radius between $2r_c = 225.10$ mm and $2r_c = 241.48$ mm. The findings demonstrating heightened vibration intensity and complex harmonic components during flow reversals suggest that future TCEC designs must incorporate advanced tooth contact optimization strategies and precision manufacturing controls to mitigate edge contact conditions under bidirectional loading. These results have significant implications for drivetrain reliability and power conversion efficiency, particularly in terms of tooth profile modifications and MS characteristics to accommodate the unique combination of high-torque loads and cyclic flow reversals that characterize tidal energy-harvesting conditions.

Author Contributions: Conceptualization, methodology and writing: D.H., Y.L. and X.Z.; software and validation: D.H. and Y.L.; formal analysis, data curation: D.H.; investigation and resources: X.Z.; writing—review and editing, supervision, project administration, and funding acquisition: G.L. All authors have read and agreed to the published version of the manuscript.

Funding: This research was funded by the U.S. National Science Foundation under Grant No. 2329791.

Data Availability Statement: Data are contained within the article.

See ABS Houston, TX Letter Ref. No. 10071825 dated 14-Aug-2026

Document must be opened with Adobe to view all ABS amendments.

Acknowledgments: The authors would like to thank Zhonghou Wang for his technical support on gear experimental investigation at the University of Shanghai for Science and Technology.

Conflicts of Interest: The authors declare no conflicts of interest.

References

1. Li, G.; Zhu, W. A review on up-to-date gearbox technologies and maintenance of tidal current energy converters. *Energies* **2022**, *15*, 9236. [CrossRef]
2. Khare, V.; Khare, C.; Nema, S.; Baredar, P. *Tidal Energy Systems: Design, Optimization and Control*; Elsevier: Amsterdam, The Netherlands, 2018.
3. Li, G.; Zhu, W. Tidal current energy harvesting technologies: A review of current status and life cycle assessment. *Renew. Sustain. Energy Rev.* **2023**, *179*, 113269. [CrossRef]
4. Elasha, F.; Mba, D.; Togneri, M.; Masters, I.; Teixeira, J.A. A hybrid prognostic methodology for tidal turbine gearboxes. *Renew. Energy* **2017**, *114*, 1051–1061. [CrossRef]
5. Zhang, D.; Liu, D.; Liu, X.; Xu, H.; Wang, Y.; Bi, R.; Qian, P. Unsteady effects of a winglet on the performance of horizontal-axis tidal turbine. *Renew. Energy* **2024**, *225*, 120334. [CrossRef]
6. Zhang, Z.; Zhang, Y.; Zheng, Y.; Zhang, J.; Fernandez-Rodriguez, E.; Zang, W.; Ji, R. Power fluctuation and wake characteristics of tidal stream turbine subjected to wave and current interaction. *Energy* **2023**, *264*, 126185. [CrossRef]
7. Chen, P.; Wu, D. A review of hybrid wave-tidal energy conversion technology. *Ocean Eng.* **2024**, *303*, 117684. [CrossRef]
8. Avalos, G.O.G.; Shadman, M.; Estefen, S.F. Application of the latching control system on the power performance of a wave energy converter characterized by gearbox, flywheel, and electrical generator. *J. Mar. Sci. Appl.* **2021**, *20*, 767–786. [CrossRef]
9. Glennon, C.; Finnegan, W.; Kaufmann, N.; Meier, P.; Jiang, Y.; Starzmann, R.; Goggins, J. Tidal stream to mainstream: Mechanical testing of composite tidal stream blades to de-risk operational design life. *J. Ocean Eng. Mar. Energy* **2022**, *8*, 163–182. [CrossRef] [PubMed]
10. Wang, Q.; Zhou, C.; Gui, L.; Fan, Z. Optimization of the loaded contact pattern of spiral bevel and hypoid gears based on a kriging model. *Mech. Mach. Theory* **2018**, *122*, 432–449. [CrossRef]
11. Liu, S.; Song, C.; Zhu, C.; Liang, C.; Yang, X. Investigation on the influence of work holding equipment errors on contact characteristics of face-hobbed hypoid gear. *Mech. Mach. Theory* **2019**, *138*, 95–111. [CrossRef]
12. Liang, C.; Song, C.; Zhu, C.; Liu, S.; Yang, X. Investigation of the effects with linear, circular and polynomial blades on contact characteristics for face-hobbed hypoid gears. *Mech. Mach. Theory* **2020**, *146*, 103739. [CrossRef]
13. Cooley, C.G.; Liu, C.; Dai, X.; Parker, R.G. Gear tooth mesh stiffness: A comparison of calculation approaches. *Mech. Mach. Theory* **2016**, *105*, 540–553. [CrossRef]
14. Huang, D.; Wang, Z.; Kubo, A. Hypoid gear integrated wear model and experimental verification design and test. *Int. J. Mech. Sci.* **2020**, *166*, 105228. [CrossRef]
15. Simon, V.V. Grinding of hypoid gears by applying generating and Waguri motions. *Mech. Mach. Theory* **2023**, *179*, 105100. [CrossRef]
16. Shi, Z.; Li, S. Nonlinear dynamics of hypoid gear with coupled dynamic mesh stiffness. *Mech. Mach. Theory* **2022**, *168*, 104589. [CrossRef]
17. Liu, Y.; Chen, L.; Mao, X.; Shangguan, D. A semi-analytical loaded contact model and load tooth contact analysis approach of ease-off spiral bevel gears. *Machines* **2024**, *12*, 623. [CrossRef]
18. Wang, J.; Lim, T.C.; Li, M. Dynamics of a hypoid gear pair considering the effects of time-varying mesh parameters and backlash nonlinearity. *J. Sound Vib.* **2007**, *308*, 302–329. [CrossRef]
19. Karagiannis, I.; Theodossiades, S. An alternative formulation of the dynamic transmission error to study the oscillations of automotive hypoid gears. *ASME J. Vib. Acoust.* **2014**, *136*, 011001. [CrossRef]
20. Mohammadpour, M.; Theodossiades, S.; Rahnejat, H. Multiphysics investigations on the dynamics of differential hypoid gears. *ASME J. Vib. Acoust.* **2014**, *136*, 041007. [CrossRef]
21. Athanasopoulos, E.; Salpistis, C.; Mohammadpour, M.; Mihailidis, A.; Theodossiades, S.; Grekoussis, R. Calculation of the kinematics of hypoid gears towards developing a method for an equivalent crossed helical gear pair selection for use in tribological experimental evaluations. *Proc. Inst. Mech. Eng. Part K J. Multi-Body Dyn.* **2017**, *231*, 519–537. [CrossRef]
22. Song, C.; Bai, H.; Zhu, C.; Wang, Y.; Feng, Z.; Wang, Y. Computational investigation of off-sized bearing rollers on dynamics for hypoid gear-shaft-bearing coupled system. *Mech. Mach. Theory* **2021**, *156*, 104177. [CrossRef]
23. Huangfu, Y.; Zhao, Z.; Ma, H.; Han, H.; Chen, K. Effects of tooth modifications on the dynamic characteristics of thin-rimmed gears under surface wear. *Mech. Mach. Theory* **2020**, *150*, 103870. [CrossRef]
24. Zheng, X.; Luo, W.; Hu, Y.; He, Z.; Wang, S. Analytical approach to mesh stiffness modeling of high-speed spur gears. *Int. J. Mech. Sci.* **2022**, *224*, 107318. [CrossRef]

SoC ABS Houston TX Letter for MOOR7A525 dated 14-Aug-2025

Document must be opened with Adobe to view all ABS amendments.

25. Li, G.; Zhu, W. An active ease-off topography modification approach for hypoid pinions based on a modified error sensitivity analysis method. *ASME J. Mech. Des.* **2019**, *141*, 093302. [CrossRef]
26. An, L.; Zhang, L.; Qin, S.; Lan, G.; Chen, B. Mathematical design and computerized analysis of spiral bevel gears based on geometric elements. *Mech. Mach. Theory* **2021**, *156*, 104131. [CrossRef]
27. Shen, Z.; Qiao, B.; Yang, L.; Luo, W.; Yang, Z.; Chen, X. Fault mechanism and dynamic modeling of planetary gear with gear wear. *Mech. Mach. Theory* **2021**, *155*, 104098. [CrossRef]
28. Yi, Y.; Huang, K.; Xiong, Y.; Sang, M. Nonlinear dynamic modelling and analysis for a spur gear system with time-varying pressure angle and gear backlash. *Mech. Syst. Signal Process.* **2019**, *132*, 18–34. [CrossRef]
29. Wei, S.; Chu, F.L.; Ding, H.; Chen, L.Q. Dynamic analysis of uncertain spur gear systems. *Mech. Syst. Signal Process.* **2021**, *150*, 107280. [CrossRef]
30. Li, G.; Zhu, W. Control and flume flow experiments of a tidal current energy converter with an infinitely variable transmission. *IEEE/ASME Trans. Mechatron.* **2024**, *29*, 2803–2811. [CrossRef]
31. Liu, Y.; Chen, L.; Li, G. Multi-points control for face-milled spiral bevel gears with a predesigned fourth-Order motion curve. *Machines* **2024**, *12*, 34. [CrossRef]
32. Chang, L.; Liu, G.; Wu, L. A robust model for determining the mesh stiffness of cylindrical gears. *Mech. Mach. Theory* **2015**, *87*, 93–114. [CrossRef]

Disclaimer/Publisher's Note: The statements, opinions and data contained in all publications are solely those of the individual author(s) and contributor(s) and not of MDPI and/or the editor(s). MDPI and/or the editor(s) disclaim responsibility for any injury to people or property resulting from any ideas, methods, instructions or products referred to in the content.

See ABS Houston, TX Letter ref WO067195 dated 14-Aug-2026